Microfluidics and Nanofluidics (2023) 27:56
https://doi.org/10.1007/s10404-023-02667-y

RESEARCH

Synthesis of gold nanoparticles with different sizes and morphologies using a single LTCC-based microfluidic system for point-of-care use in personalized medicine

Natália Cristina Dalibera[1,2] · **Aline Furtado Oliveira**[3] · **Adriano Rodrigues Azzoni**[2]

Received: 3 February 2023 / Accepted: 24 July 2023 / Published online: 31 July 2023

Abstract

The potential of microfluidics for *point-of-care* diagnosis and personalized medicine has been drawing attention to this technology in biomedical fields. Low Temperature Co-Fired Ceramics (LTCC) is a promising material for the construction of microfluidic systems for *point-of-care* use since it has favorable inherent physico-chemical properties, and its fabrication methods are simple and easy to adapt to further needs. Here, we design and construct a microdevice for the continuous synthesis of gold nanoparticles (AuNPs), based on reduction using modified citrate protocols. The AuNPs produced were characterized using Transmission Electron Microscopy (TEM), Dynamic Light Scattering (DLS), and Zeta Potential analysis. Depending on the temperature, residence time, and citrate concentration chosen during synthesis, a range of nanoparticle sizes and shapes were consistently produced, indicating that the process could be suitable for the production of nanoparticles for personalized medicine. By using a single microreactor, AuNPs were produced with sizes ranging from 19 to 117 nm, with at least 7 different shapes, including complex morphologies, such as nanodendrites and tadpole-shaped particles, indicating the simplicity and versatility of the microfluidic device.

Graphical abstract

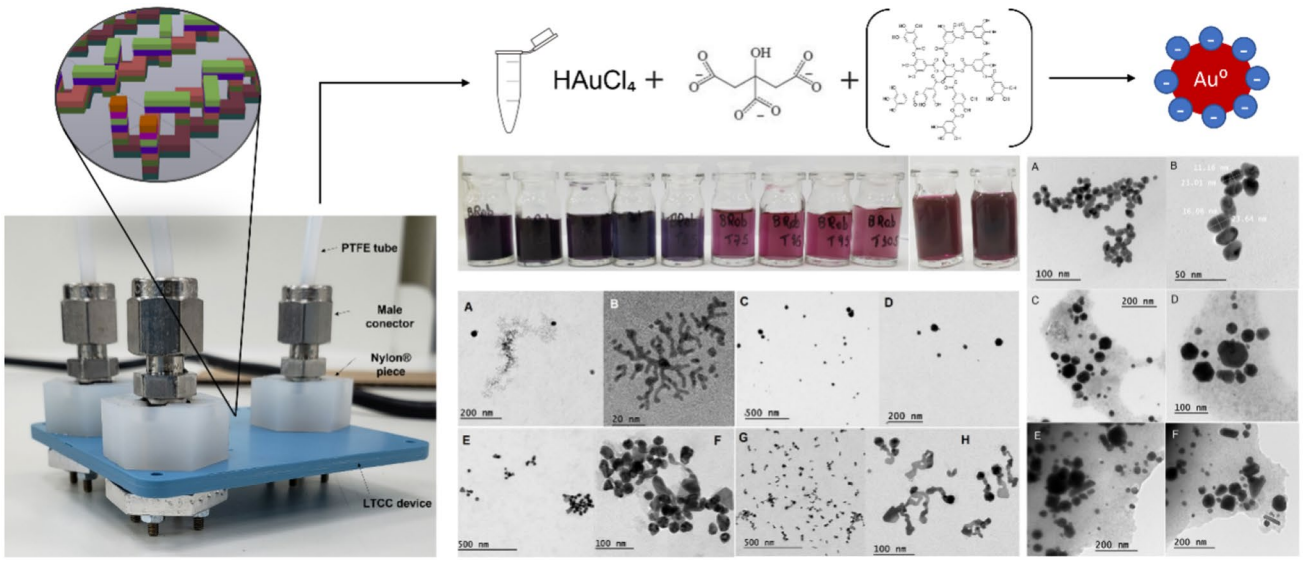

Keywords Low temperature co-fired ceramics · Microfluidics · Gold nanoparticles · Personalized medicine

Extended author information available on the last page of the article

1 Introduction

Microfluidics is a multidisciplinary field in which small amounts of fluids are processed. Microfluidic devices exploit hydrodynamic characteristics to control the organization of different molecules within microchannels (Whitesides 2006). The advantages of microfluidic systems over conventional systems include faster reactions, minimal device size, lower sample and reagent consumption, precise control of energy and mass transfer phenomena, low energy consumption and dissipation, and low relative cost of production per device (Li 2008). Mainly due to their small size, the microfluidic devices can be used according to the recent perspectives of personalized medicine, such as gene therapy and immunotherapies (Whitesides 2006). For these applications, *point-of-care* use can facilitate therapeutic treatment, reducing the amount of oxidized and degraded compounds. The potential of microfluidics for *point-of-care* diagnosis has been drawing attention in biomedical fields (Sista et al. 2008; Linder 2007). Microfluidics offers the potential to satisfy all the main demands for an ideal *point-of-care* system: portability, biocompatibility, low cost per unit and the ability to deliver instantaneous results (Gervais et al. 2011; Vasudev et al. 2013).

Microfluidic devices can be fabricated using different classes of materials, including glass, silicon and different polymers (Becker and Locascio 2002; Bilitewski et al. 2003; Chan et al. 2003, 2005). However, many employed micro-manufacturing techniques require a post-fabrication sealing that may produce leaks and may exhibit poor chemical and thermal inertness and slow prototyping procedures (Gómez-De Pedro et al. 2010; Leatzow et al. 2002). For this reason, low temperature co-fired ceramics (LTCC) has gained attention as an alternative material for fabrication of microfluidics systems (Vasudev et al. 2013; Gongora-Rubio et al. 2001; Golonka et al. 2011).

LTCC-based fabrication of microdevices consists of the parallel processing of multiple layers and final integration into a multilayer stack, which facilitates the design modification during initial development. The multilayer approach not only allows the incorporation of 3-D structures, but also results in a leak-free compact device (Vasudev et al. 2013). The relatively simple and inexpensive fabrication methods, fast prototyping, and the low turn-around time in a semi-clean room environment with minimal use of expensive tools significantly reduce the cost and production time of LTCC microfluidic systems. Furthermore, LTCC inherent properties offer a number of advantages over polymers and glass, such as chemical inertness, biocompatibility, high-temperature and pressure stability, excellent high frequency dielectric properties, mechanical strength and corrosion resistance (Vasudev et al. 2013; Gómez-De Pedro et al. 2010; Shafique and Robertson 2009).

LTCC microdevices have been used to synthesize nanoparticles made of a large range of materials, such as metals, polymers and biomolecules (Gongora-Rubio et al. 2001, 2013; Schianti et al. 2013; Gomez et al. 2018; Hung and Lee 2007). Nanoparticles show unique properties based on their composition, size, shape and morphology; thus methods and devices that enable a fine control of the synthesis are highly pursued to achieve desired characteristics (Hung and Lee 2007). In the past few years, many nanoparticles have been developed for biomedical applications (Ma et al. 2017; Hao et al. 2018; Li et al. 2017), highlighting gold nanomaterials as especially promising (Wang et al. 2015; Singh et al. 2018; Liu et al. 2014; Salazar-González et al. 2015; Dykman 2020). The tunable shape, size and surface characteristics of gold nanoparticles (AuNPs), along with their excellent biocompatibility, render them ideal candidates for applications in biomedical imaging, biological sensing, drug and gene delivery, vaccines and photothermal therapy, among other purposes (Sasidharan and Monteiro-riviere 2015).

Gold nanoparticles of different sizes, ranging from 5 nm (Paquin et al. 2015) to 1 μm (Zhang et al. 2003), and different morphologies, such as spheres (Niikura et al. 2013), rods (Uson et al. 2016), dendritic particles (Iost et al. 2019), cubes (Thiele et al. 2016), hexagons (Weng et al. 2008) and chiral particles (Xu et al. 2022), have been applied to biomedicine. Although great progress has been made in synthesizing AuNPs with high degree of monodispersity, the synthesis of these particles with different sizes and aspect ratios still requires a complicated tuning process (Ye et al. 2020). The expensive process of preparing the growth solution and the structural instability of the gold seeds result in limitation of yield, shape and reproducibility of AuNPs colloids, which has greatly hampered their potential for practical applications (Ye et al. 2020). To overcome these limitations, automated and miniaturized continuous flow methods have been recently proposed to allow rapid, controlled and precise adjustment of most required experimental variables (Gómez-De Pedro et al. 2010). Moreover, simple and robust microfluidic systems make it possible to obtain AuNPs with desired properties on demand (De Mello et al. 2004; Lin et al. 2004; Wagner et al. 2004).

In this study, we present a simple-to-use, inert, robust, portable, LTCC-based microfluidic system able to produce a variety of AuNPs of different sizes and shapes on demand in a single device, making it ideal for *point-of-care* uses, in personalized medicine.

2 Materials and methods

2.1 Reagents

During the conduction of the experiments, ultrapure water, tannic acid (Sigma-Aldrich, analytical grade), sodium citrate dihydrate (NaCt) (Sigma-Aldrich, purity ≥ 99%) and gold(III) chloride trihydrate (Sigma-Aldrich, purity ≥ 99.9%) were used. All other chemicals used in this work were at least analytical grade.

2.2 Microfluidic system

The microdevice used in this study was made of *DuPont Green Tape 951PX*LTCC with a raw thickness of 254 ± 13 µm, with a X,Y shrinkage coefficient of 12.7 ± 0.3 µm and a Z shrinkage coefficient of 15 ± 0.5 µm, density of 3.1 g/cm^3 and thermal conductivity of 3.3 W/m.K. The device was composed of stacked LTCC layers, which were designed using AutoCAD® software version 2021. The device is divided into two sections: heating section (top layers) and reaction section (bottom layers), as seen in Fig. 1. There is no mixing of the inlet fluids in the heating section, its purpose is to allow the currents to reach desired temperature before the mixing. The reaction section is where the synthesis actually occurs. It features cross-channel geometry with a volume of 270 µL and 400 µm width square-base channels. The residence time of the fluids within the device starts when the currents enter the reaction section.

The ceramic sheets were cut using a *LPKF Laser & Electronics* laser printer model *Proto Laser U3*. After cutting, the lamination step was carried out, in which the layers were stacked in order and aligned on a metallic support. The material was then kept in a *Sppencer Scientific* oven model *SP2420-12* at 60 ℃ for 20 min. After that, the sheets were pressed together by a hydraulic press, at 70 ℃ and 4 tons for 20 min. Then, the device was subjected to the sintering process. At this stage, the microdevice was removed from the metallic support and placed on a porous ceramic platform, in which it was taken to an *EDG Equipamentos* muffle furnace model *FCVE-II*. Inside the muffle, the material was subjected to a temperature ramp of 6 ℃/min to 450 ℃, remaining at this temperature for 60 min. Then, the temperature was raised to 850 ℃, again at a rate of 6 ℃/min, remaining at this temperature for another 60 min. After the complete sintering of the material, the device was left overnight inside the muffle to cool down.

In order to construct the experimental setup (microreactor device) for the synthesis of gold nanoparticles, hydraulic connection adaptors and other apparatus were assembled. The connections for the tubes were custom made using

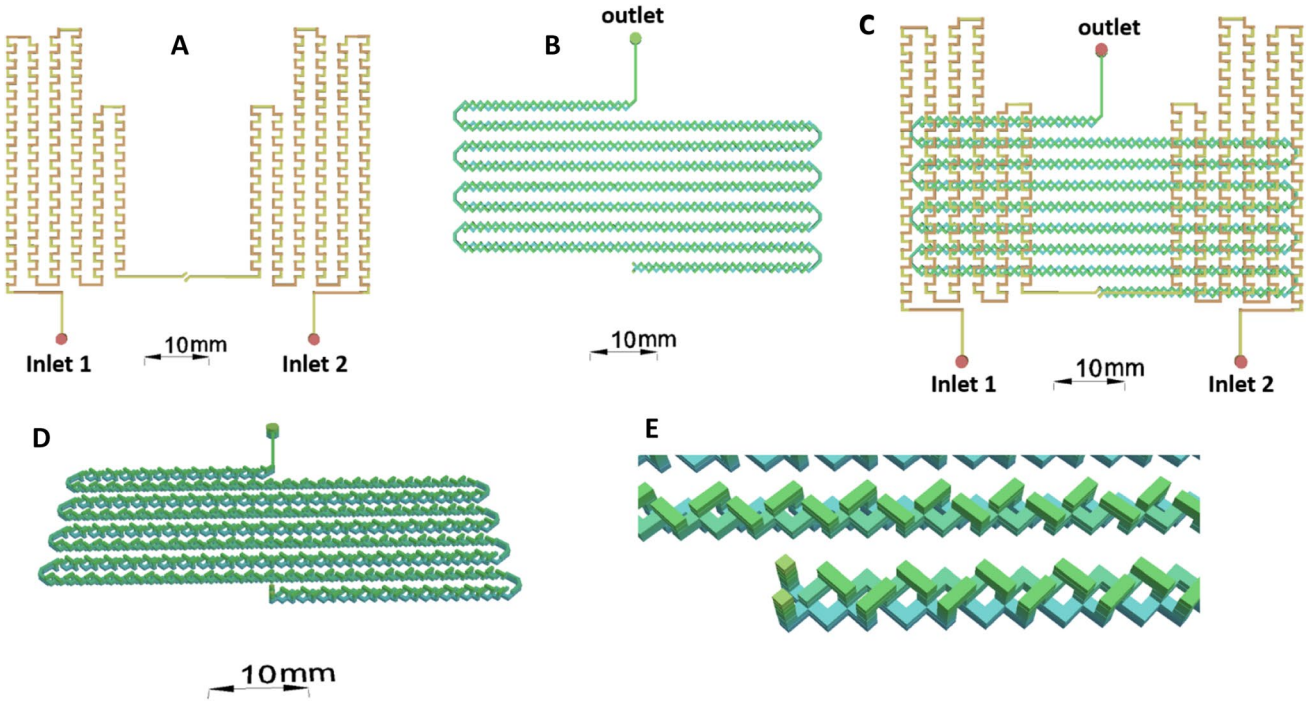

Fig. 1 3D scheme of the microdevice. **A** Top view of the heating section; **B** top view of the reaction section; **C** top view of both heating section (top layers) and reaction section (bottom layers); **D** side view of the reaction section; **E** closer side view of the cross-channel geometry of the channels in the reaction section

3 pairs of pieces of polyamide 6 (Nylon®) and 3 pairs of rubber *o-rings* attached to the device with screws. A *Swagelok* 316 stainless steel double ferrule male connector was threaded into each piece attached to the reactor, securing the *Darwin* 1/8″ OD and 1/16″ ID PTFE tubes. The free ends of the inlet tubes were connected to 5 mL luerlock plastic syringes. The syringes were attached to a *Harvard Apparatus* syringe pump model *PHD 2000*. The device was immersed in a *PolyScience* oil bath model *SD07H170-A12E* for temperature control. Images of the device after the sintering process, the assemble of the microfluidic system and the assemble of the whole experimental apparatus are shown in Fig. 2.

2.3 Synthesis of gold nanoparticles

For the synthesis of gold nanoparticles, two series of studies were performed: the first one used sodium citrate (NaCt) as reducing and stabilizing agent, varying the reaction temperature from 25 to 100 ℃; the second one used tannic acid as the main reducing agent, with different amounts of NaCt as the stabilizing agent at room temperature. For the first series of tests, a 2.5 mM gold chloride solution in ultrapure water (precursor solution) and a 7.5 mM NaCt solution in ultrapure water (reducing solution), were prepared in order to keep the NaCt to Gold molar ratio at 3:1 (Cardoso 2018). The syntheses were carried out at temperatures of 25 ℃, 35 ℃, 45 ℃, 55 ℃, 65 ℃, 75 ℃, 85 ℃, 95 ℃ and 100 ℃, respectively. For the second series of tests, the same precursor solution containing 2.5 mM gold chloride was used. The reducing solution, this time, contained 0.1 mM of tannic acid with different amounts of NaCt (1.25 mM, 2.5 mM, 5.0 mM and 7.5 mM, respectively). All the syntheses using tannic acid were carried out at 25 ℃. All reactions were performed in triplicate using the same device, adjusting the flow rate of the pumps in order to set the residence time at 90 s. The precursor and reducing solutions entered the device at different inlets at the same flow rate (0.18 mL.min^{-1}). The reaction products were stored for 24 h at room temperature before the characterization.

2.4 Dynamic light scattering (DLS) and zeta potential analysis

Particle size analyses were performed using the Dynamic Light Scattering (DLS) technique at 25 ℃, in a glass cuvette,

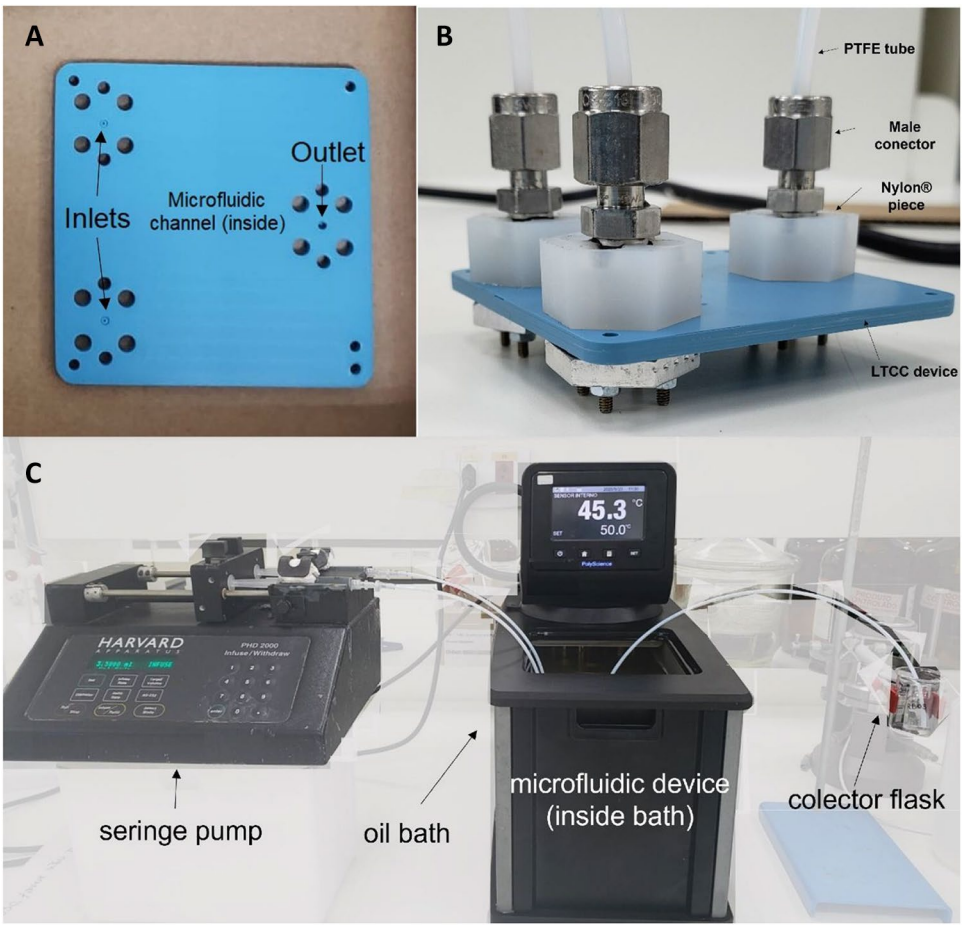

Fig. 2 Experimental apparatus. **A** Microdevice after the sintering process; **B** assemble of the microfluidic system connected to the PTFE tubes; **C** assemble of the experimental apparatus

with a *Particulate Systems NanoPlus* equipment. Samples were diluted to 10% in ultrapure water and each reading was performed in triplicate. The surface charge of the particles in water was assessed through zeta potential analysis with the same *NanoPlus* equipment at 25 ℃. Samples were diluted to 10% in ultrapure water and readings were taken at 5 different points with 10 readings per point for each sample.

2.5 Transmission electron microscopy (TEM)

TEM analyses were performed using a transmission electron microscope *JEOL JEM 2100* (JEOL, USA). The samples were dripped onto a formvar/carbon supported copper grid mash 300. The microscopy images obtained were analyzed using Image J software. Statistical analyzes were performed using Minitab 19.1.1 software, considering a sample number $n \geq 300$ and the average based on 3 images from distinct regions of each triplicate.

3 Results and discussion

As expected for any newly designed microreactor device, a series of preliminary experiments were first conducted to determine the ideal reaction parameters in order to maximize the conversion during the synthesis of the gold nanoparticles. These experiments lead to a fixed residency time of 90 s and concentration of reactant fixed at 2.5 mM for the gold precursor solution. The results of these studies are shown and discussed in the Supplementary Information of this article. Following these preliminary studies, a series of synthesis experiments were performed using 7.5 mM NaCt as a reducing and stabilizing agent and varying only the temperature of the synthesis. The results of size, zeta potential and polydispersity are shown in Table 1.

We observed that the higher the temperature of the synthesis, the bigger the size of the synthesized particles for temperatures up to 75 ℃. For temperatures higher than 75 ℃, the AuNPs showed no significant difference in size. On the other hand, PD values showed a similar behavior in the contrary direction: the higher the temperature, the smaller the PD up to 85 ℃, as shown in Fig. 3A. All PD values obtained, however, were up to 0.35, showing low polydispersity. The conversion of gold salt to AuNPs, assessed using an indirect methodology (Haiss et al. 2007), was > 95% for all the synthesis studied, as shown in the Supplementary Information. These results reveal that it was possible to tune the size of AuNPs synthesized using the microdevice, from 19 to 117 nm, by simply altering the temperature of the process. All particles show negative surface charge, as it is expected from AuNPs synthesized using NaCt as the only reducing agent (Park and Shumaker-Parry 2014), and good colloidal stability, evidenced by zeta potential values lower than − 30 mV (Malvern Ltd. 2011). Furthermore, macroscopic characteristics such as color varies among the AuNPs produced. The particles synthesized at temperatures from 25 to 45 ℃ showed a deep dark purple color, while the synthesis at 60 ℃ resulted in a dark blue color. Finally, those particles produced at temperatures from 75 to 100 ℃ turned out pink, as seen in Fig. 3B.

Table 1 Results of size, zeta potential and polydispersity (PD) for the products of syntheses carried out using NaCt as reducing and stabilizing agent, varying only the temperature of the synthesis from 25 to 100 ℃

Temperature (℃)	Size (nm)	Zeta potential (mV)	PD
25	19.1 ± 0.17	− 45.60 ± 0.16	0.35
30	32.0 ± 0.68	− 36.46 ± 0.79	0.34
45	64.9 ± 0.83	− 35.12 ± 0.87	0.28
60	83.4 ± 1.85	− 34.94 ± 0.39	0.26
75	107.5 ± 0.23	− 33.37 ± 0.85	0.23
85	106.4 ± 2.19	− 35.61 ± 0.49	0.21
95	108.4 ± 0.82	− 37.43 ± 0.24	0.22
100	117.1 ± 2.31	− 32.60 ± 0.61	0.25

The color difference among AuNPs may be explained not only by the difference in the mean hydrodynamic diameter of the particles but also by the morphology, since both size and shape directly influence the color of the colloidal suspension (Aldewachi et al. 2018). This characteristic makes AuNPs suitable for applications such as colorimetric biosensors (Aldewachi et al. 2018). For spherical AuNPs, it is usual to observe a red color in suspension, which changes to blue/purple and eventually progresses to a clear color with precipitates upon aggregation (McFarland et al. 2004). However, the purple and blue colloids produced here showed good stability over time and there was no sign of precipitation. This suggests that maybe the morphology of the particles were responsible for the non-red color displayed, as previously reported in the literature (Zhang et al. 2016), instead of their state of aggregation. To prove that hypothesis, samples of products of syntheses performed at 25 ℃, 60 ℃ and 95 ℃ were observed by TEM, and the results are shown in Fig. 4.

The synthesis carried out at 25 ℃ resulted in oval AuNPs with mean aspect ratio (R/r) of 2. The product of the synthesis performed at 60 ℃ showed the presence of particles with different morphologies, with predominance of 59.4% hexagon-like shapes. For the synthesis carried out at 95 ℃, the results show particles with many different morphologies such as spheres, rods, hexagons and triangles mixed together. Unlike the products usually obtained in bulk synthesis of AuNPs from gold chloride and NaCt (Dong et al. 2020; Kimling et al. 2006; Wuithschick et al. 2015), it is common to obtain non-spherical particles by microfluidic routes (Ye et al. 2020; Abalde-Cela et al. 2018; Calamak and

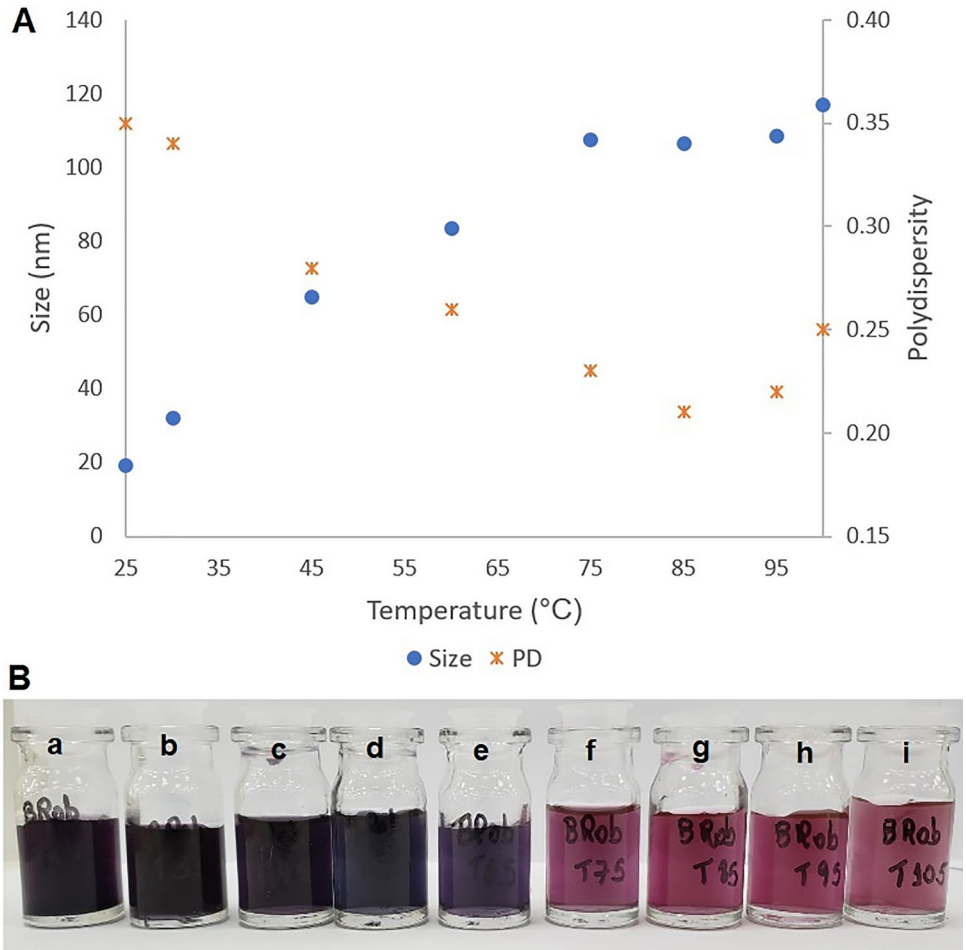

Fig. 3 Synthesis of gold nanoparticles (AuNPs) using the microdevice at different reaction temperatures. The syntheses were carried out using NaCt as reducing and stabilizing agent. **A** Results of the size (blue circles) and polydispersity (orange asterisks) of the AuNPs. **B** Macroscopic appearance of the different AuNPs produced at (a) 25 ℃; (b) 30 ℃; (c) 45 ℃; (d) 60 ℃; (e) 65 ℃; (f) 75 ℃; (g) 85 ℃; (h) 95 ℃; (i) 100 ℃ (Color figure online)

Ulubayram 2019). The reason behind this is not completely elucidated, however there are reported mechanisms that use the hypothesis that larger nanostructures of a variety of shapes are formed by the fusion of smaller triangular nanoparticles that are randomly synthesized (Wagner et al. 2004; Jana et al. 2001; Mukherjee et al. 2002; Jin et al. 2003). It is known that the precise control of process variables enabled by microfluidic technologies makes it possible to obtain high quality non-spherical metal nanoparticles, giving scientists new insights for the development of particles with desired characteristics (Köhler and Knauer 2017).

In order to further investigate if it would be possible to obtain even more types of AuNPs using the same assembled microfluidic device and the same reaction conditions (same residency time of 90 s and same 2.5 mM precursor solution, now with fixed temperature of 25 ℃), we studied the synthesis with tannic acid 0.1 mM mixed with different amounts of NaCt as the reducing solution. The results of size, zeta potential and polydispersity and the macroscopic appearance of the products of syntheses with tannic acid are shown in Table 2 and Fig. 5, respectively.

The colors of the AuNPs produced using tannic acid with NaCt varied from deep red (for NaCt 1.3 mM) to deep dark purple (for NaCt 7.5 mM). The use of higher concentrations of NaCt not only decreased the mean hydrodynamic diameter of the particles (from 85.7 to 21.6 nm for NaCt at 1.3 mM and 7.5 mM, respectively), but also increased the module of their zeta potential (from 35.07 to 46.47 mV for NaCt at 1.3 mM and 7.5 mM, respectively), indicating that the excess of NaCt makes the colloid suspension more stable, probably due to a larger layer of citrate molecules (negatively charged) protecting the particles from aggregation as a consequence of electric repulsion. However, all colloids showed good stability even with low NaCt concentration, since all results for zeta potential are lower than − 30 mV. Both AuNPs synthesized using tannic acid with NaCt at 1.3 mM and using only NaCt at reaction temperature of 60 ℃ showed similar mean particle size (85.7 nm and 83.4 nm, respectively) but presented different suspension color (Figs. 4B–D and 5A, respectively), indicating that the shape of the particles varied between them. To verify the morphologies of the AuNPs produced in the second series of tests, samples were observed by TEM, and the results are shown in Fig. 6. The conversions of gold salt to AuNPs were also > 95% for all the synthesis in this series, as shown in the Supplementary Information.

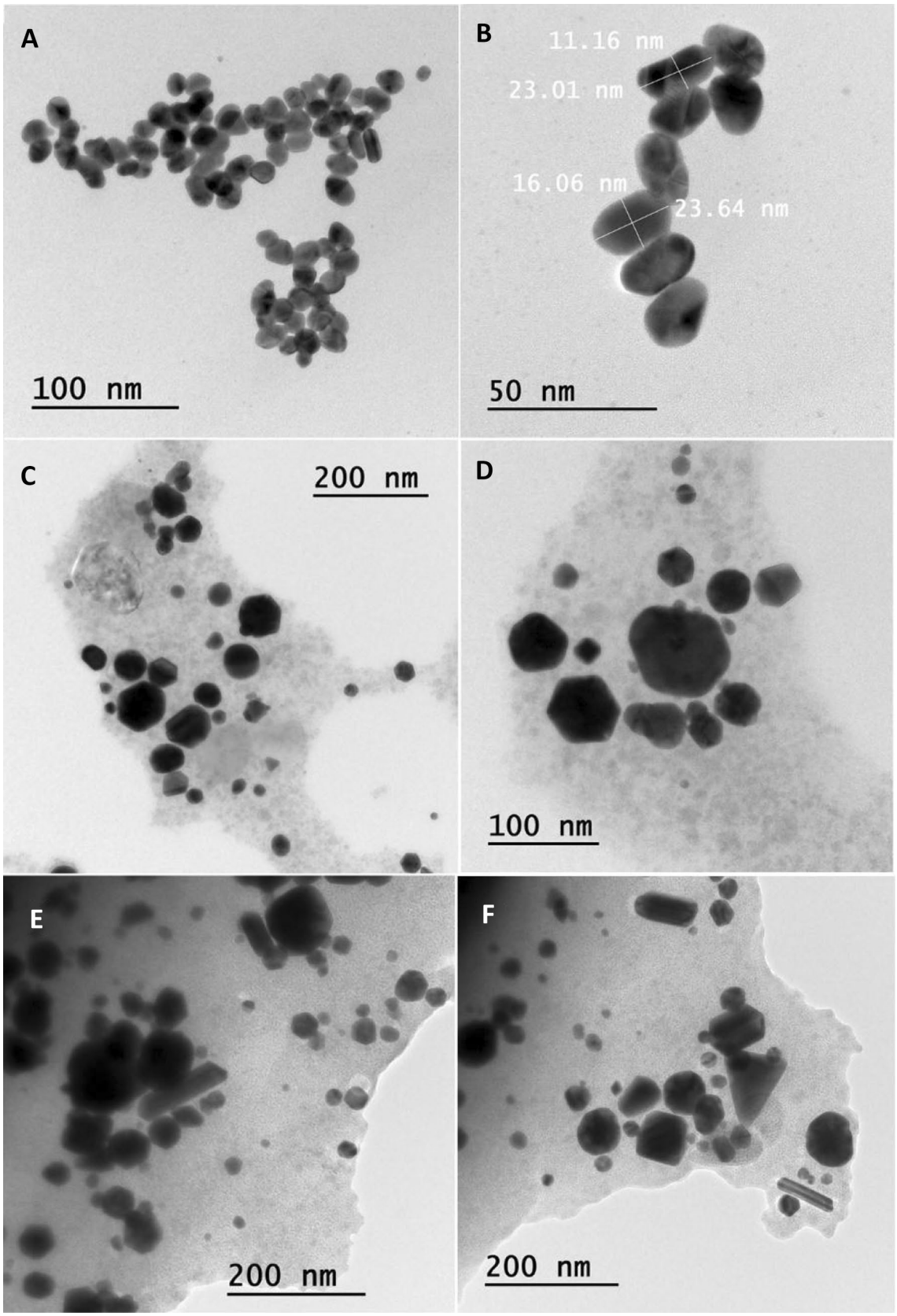

Fig. 4 TEM images of AuNPs produced using NaCt as reducing and stabilizing agent, for reactions carried out at: **A** and **B** 25 ℃; **C** and **D** 60 ℃; **E** and **F** 95 ℃

Table 2 Results of size, zeta potential and polydispersity for the products of syntheses carried out using tannic acid mixed with different amounts of NaCt as reducing solution, varying NaCt concentration from 1.3 to 7.5 mM

NaCt concentration (mM)	Size (nm)	Zeta potential (mV)	PD
1.3	85.7 ± 0.21	−35.07 ± 1.20	0.207
2.5	79.5 ± 1.19	−42.22 ± 1.91	0.225
5.0	47.2 ± 0.76	−44.84 ± 1.65	0.323
7.5	21.6 ± 0.61	−46.77 ± 2.09	0.344

The synthesis carried out using tannic acid with NaCt 1.3 mM resulted predominantly in dendritic AuNPs with different degrees of ramification (Fig. 6A and B). Variations of this particular morphology have been seen before in the literature and have the potential to be used in electronics and sensing applications (Iost et al. 2019; Calamak and Ulubayram 2019; Uppal et al. 2013). Reactions with NaCt 2.5 mM resulted mostly in spheres with a mean diameter of 79.5 nm (Fig. 6C and D). The synthesis carried out using NaCt 5.0 mM resulted in irregular shapes with no predominant morphology (Fig. 6E and F). Finally, syntheses carried out with tannic acid and NaCt 7.5 mM produced tadpole-shaped particles (Fig. 6G and H). Tadpole-shaped AuNPs have been reported in literature before (Wu et al. 2012; Bai et al. 2009; Li et al. 2013; Hu et al. 2004) and there is evidence that this particular structure may be the result of the ripening of particles with other morphologies (Wu et al. 2012). Reports applying tadpole-shaped AuNPs are scarce, however the synthesis of novel metallic nanostructures are important since they may exhibit a wide range of unique

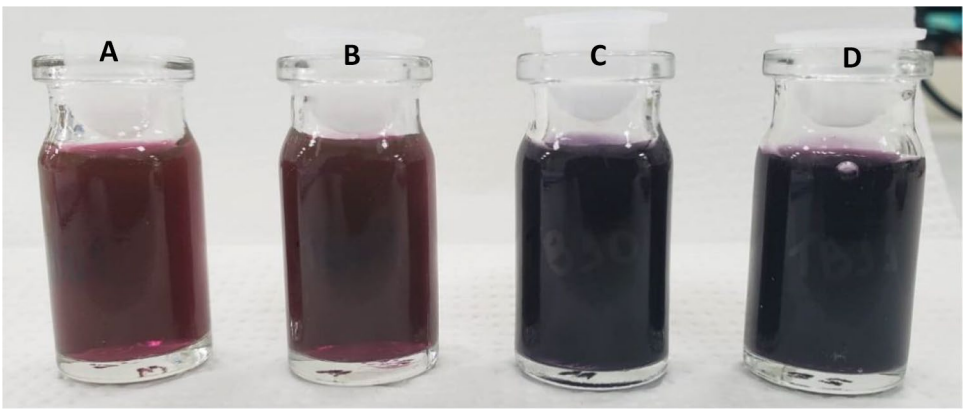

Fig. 5 Macroscopic appearance of the products of syntheses carried out using tannic acid mixed with different amounts of NaCt as reducing solution, varying NaCt concentration in **A** 1.3 mM; **B** 2.5 mM; **C** 5.0 mM; **D** 7.5 mM

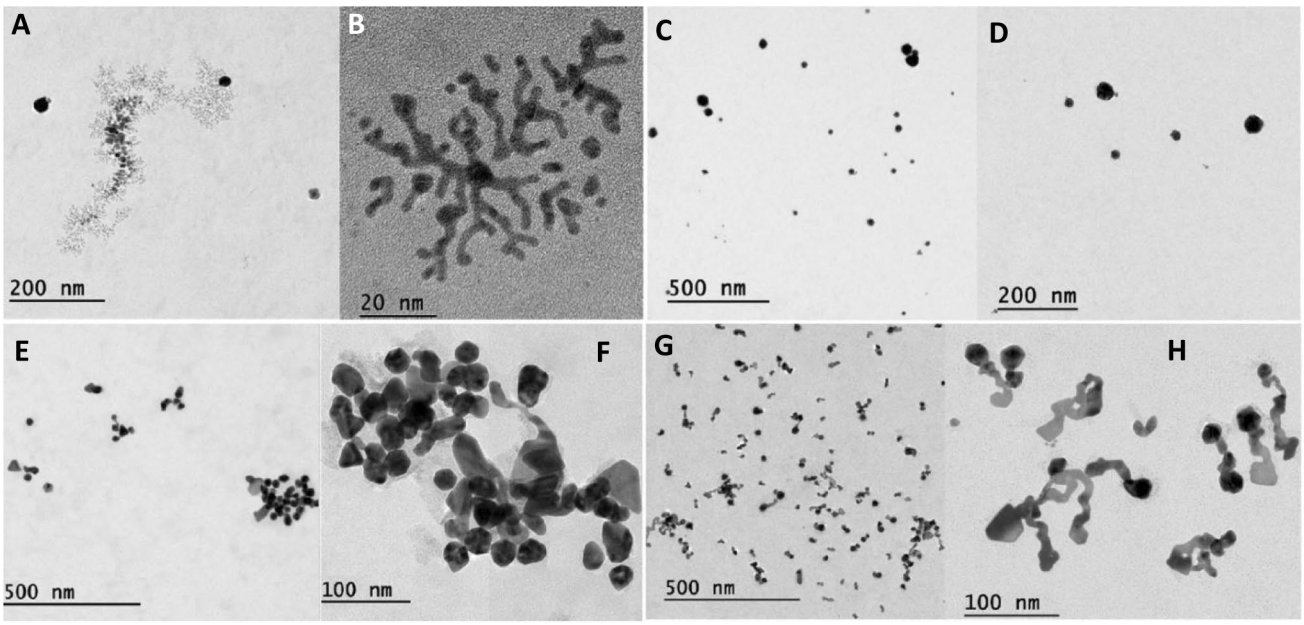

Fig. 6 TEM images of products of syntheses carried out using tannic acid mixed with different amounts of NaCt as reducing solution, varying NaCt concentration in: **A** and **B** 1.3 mM; **C** and **D** 2.5 mM; **E** and **F** 5.0 mM; **G** and **H** 7.5 mM

electrical and optical properties and may find applications in a variety of areas, such as nanodevices, biomaterials, electrochemistry and so on (Li et al. 2013; Hu et al. 2004).

4 Conclusion

We have developed an LTCC-based microfluidic system that is simple, low-cost, low-maintenance, chemically inert, portable, and robust for *point-of-care* use. Utilizing a single device, with just a few adjustments in the process, we demonstrated that it is possible to synthesize stable AuNPs of different colors, sizes and shapes, including complex morphologies such as nanodendrites and tadpole-shaped particles, in a controlled and reproducible way, thus being ideal for applications in personalized medicine.

It is possible to adapt the technology presented in this study adding, for example, sensors for online monitoring of the reaction and sections for inline functionalization of the synthesized particles. Furthermore, we believe that it is possible to produce AuNPs with even more sizes and morphologies by altering other process parameters, such as retention time, nature and concentration of reagents and pH. In the future, we intend to evaluate the cytotoxicity, surface characteristics and interaction of the synthesized AuNPs with different biomolecules (e.g. proteins and mRNA) providing new applications of the functionalized nanoparticles in advanced vaccines, therapies, and diagnostics.

Supplementary Information The online version contains supplementary material available at https://doi.org/10.1007/s10404-023-02667-y.

Acknowledgements We would like to thank the *Institute for Technological Research (IPT)* where the microfluidic device was constructed and where the experiments were carried out.

Author contributions Ideation and design of the experiments were performed by NCD, AFO and ARA; collection of experimental data was done by NCD; analysis of experimental data were done by NCD, AFO and ARA; NCD drafted the core of the manuscript, whereas AFO and ARA improved, edited and added to various sections of the text. All authors read and approved the final manuscript.

Funding This work was supported by CNPq—Conselho Nacional de Desenvolvimento Científico e Tecnológico (grants 305747/2020-7, 444412/2014-0, 307739/2015-5 and 304125/2018-0). The authors also acknowledge the financial support of the Coordenação de Aperfeiçoamento de Pessoal de Nível Superior—Brazil (CAPES/PROEX)—Finance Code 001.

Availability of data and materials The authors state that all data underlying the findings are fully available without restriction. All relevant data are within the paper.

Declarations

Conflict of interest The authors declare no competing interests.

Ethical approval This article does not contain studies with human participants or animals. Hence, no formal consent is required.

Consent to participate Consent was obtained from all individual participants included in this study.

Consent to publish All the participants have consented to the submission of this article.

References

Abalde-Cela S, Taladriz-Blanco P, Oliveira MGD, Abell C (2018) Droplet microfluidics for the highly controlled synthesis of branched gold nanoparticles. Sci Rep 8(1):1–6. https://doi.org/10.1038/s41598-018-20754-x

Aldewachi H, Chalati T, Woodroofe MN, Bricklebank N, Sharrack B, Gardiner P (2018) Gold nanoparticle-based colorimetric biosensors. Nanoscale 10(1):18–33. https://doi.org/10.1039/C7NR06367A

Bai X, Zheng L, Liu H, Zhao M (2009) Synthesis of tadpole-shaped Au nanoparticles using a Langmuir monolayer of fluorocarbon surfactant. Mater Lett 63(13–14):1156–1158. https://doi.org/10.1016/j.matlet.2009.02.026

Becker H, Locascio LE (2002) Polymer microfluidic devices. Talanta 56(2):267–287. https://doi.org/10.1016/S0039-9140(01)00594-X

Bilitewski U, Genrich M, Kadow S, Mersal G (2003) Biochemical analysis with microfluidic systems. Anal Bioanal Chem 377(3):556–569. https://doi.org/10.1007/s00216-003-2179-4

Calamak S, Ulubayram K (2019) Controlled synthesis of multi-branched gold nanodendrites by dynamic microfluidic flow system. J Mater Sci 54(10):7541–7552. https://doi.org/10.1007/s10853-019-03403-0

Cardoso RM (2018) Nanopartículas multifuncionais dispersáveis e suas potenciais aplicações em nanomedicina. PhD thesis, Universidade de São Paulo, São Paulo, Brazil. https://doi.org/10.11606/T.46.2018.tde-24092018-141517

Chan EM, Mathies RA, Paul Alivisatos A (2003) Size-controlled growth of CdSe nanocrystals in microfluidic reactors. Nano Lett 3(2):199–201. https://doi.org/10.1021/nl0259481

Chan EM, Paul Alivisatos A, Mathies RA (2005) High-temperature microfluidic synthesis of semiconductor nanocrystals in nanoliter droplets. J Am Chem Soc 127:13854–13861. https://doi.org/10.1021/ja051381p

Dong Jiaqi, Carpinone Paul L, Pyrgiotakis Georgios, Demokritou Philip, Moudgil Brij M (2020) Synthesis of precision gold nanoparticles using Turkevich method. KONA Powder Part J 37:224–32. https://doi.org/10.14356/kona.2020011

Dykman LA (2020) Gold nanoparticles for preparation of antibodies and vaccines against infectious diseases. Expert Rev Vaccines 19(5):465–477. https://doi.org/10.1080/14760584.2020.1758070

Gervais L, De Rooij N, Delamarche E (2011) Microfluidic chips for point-of-care immunodiagnostics. Adv Mater. https://doi.org/10.1002/adma.201100464

Golonka L, Bembnowicz P, Malecha K (2011) Low temperature co-fired ceramics (LTCC) microsystems. Opt Appl 41(2):383–388

Gomez HC, Cardoso RM, de NovaisSchianti J, de Oliveira AM, Gongora-Rubio MR (2018) Fab on a package: LTCC microfluidic devices applied to chemical process miniaturization. Micromachines. https://doi.org/10.3390/mi9060285

Gómez-De Pedro S, Puyol M, Alonso-Chamarro J (2010) Continuous flow synthesis of nanoparticles using ceramic microfluidic devices. Nanotechnology. https://doi.org/10.1088/0957-4484/21/41/415603

Gongora-Rubio MR, Espinoza-Vallejos P, Sola-Laguna L, Santiago-Avilés JJ (2001) Overview of low temperature co-fired ceramics tape technology for meso-system technology (MsST). Sens Actuators A Phys 89(3):222–241. https://doi.org/10.1016/S0924-4247(00)00554-9

Gongora-Rubio MR, de Novais JS, Gomez HC, da Costa AT (2013) LTCC-3D coaxial flow focusing microfluidic reactor for micro and nanoparticle fabrication and production scale-out. J Microelectron Electron Packag 10(3):102–108. https://doi.org/10.4071/imaps.383

Haiss W, Thanh NTK, Aveyard J, Fernig DG (2007) Determination of size and concentration of gold nanoparticles from UV−Vis spectra. Anal Chem 79(11):4215–4221. https://doi.org/10.1021/ac0702084

Hao N, Nie Y, Zhang JXJ (2018) Microfluidic synthesis of functional inorganic micro-/nanoparticles and applications in biomedical engineering. Int Mater Rev 63(8):461–487. https://doi.org/10.1080/09506608.2018.1434452

Hu J, Zhang Y, Liu Bo, Liu J, Zhou H, Yunfeng Xu, Jiang Y, Yang Z, Tian ZQ (2004) Synthesis and properties tadpole-shaped gold nanoparticles. J Am Chem Soc 126(31):9470–9471. https://doi.org/10.1021/ja049738x

Hung LH, Lee AP (2007) Microfluidic devices for the synthesis of nanoparticles and biomaterials. J Med Biol Eng 27(1):1–6

Iost RM, Martins MVA, Crespilho FN (2019) Dendritic gold nanoparticles towards transparent and electroactive electrodes. Anais Da Academia Brasileira de Ciencias 91(4):1–13. https://doi.org/10.1590/0001-3765201920180817

Jana NR, Gearheart L, Murphy CJ (2001) Seeding growth for size control of 5–40 Nm diameter gold nanoparticles. Langmuir 17(22):6782–6786. https://doi.org/10.1021/la0104323

Jin R, Charles Cao Y, Hao E, Métraux GS, Schatz GC, Mirkin CA (2003) Controlling anisotropic nanoparticle growth through plasmon excitation. Nature 425(6957):487–490. https://doi.org/10.1038/nature02020

Kimling J, Maier M, Okenve B, Kotaidis V, Ballot H, Plech A (2006) Turkevich method for gold nanoparticle synthesis revisited. J Phys Chem B 110(32):15700–15707. https://doi.org/10.1021/jp061667w

Köhler JM, Knauer A (2017) The electric soul of metal nanoparticles—what experiments with microfluidically prepared colloids tell us. Adv Nano-Bio-Mater Devices 1(1):1–17

Leatzow DM, Dodson JM, Golden JP, Ligler FS (2002) Attachment of plastic fluidic components to glass sensing surfaces. Biosens Bioelectron 17(1–2):105–110. https://doi.org/10.1016/S0956-5663(01)00250-0

Li D (2008) Encyclopedia of microfluidics and nanofluidics. Compr Nanosci Nanotechnol. https://doi.org/10.1016/B978-0-12-812295-2.00132-X

Li F, Tian D, Cui H (2013) Synthesis and characterizations of isoluminol-functionalized, tadpole-shaped, gold nanomaterials. Luminescence 28(1):7–15. https://doi.org/10.1002/bio.1380

Li LL, Li X, Wang H (2017) Microfluidic synthesis of nanomaterials for biomedical applications. Small Methods 1(8):1–9. https://doi.org/10.1002/smtd.201700140

Lin XZ, Terepka AD, Yang H (2004) Synthesis of silver nanoparticles in a continuous flow tubular microreactor. Nano Lett 4(11):2227–2232. https://doi.org/10.1021/nl0485859

Linder V (2007) Microfluidics at the crossroad with point-of-care diagnostics. Analyst 132(12):1186–1192. https://doi.org/10.1039/b706347d

Liu X, Li W-J, Li L, Yang Y, Mao L-G, Peng Z (2014) A label-free electrochemical immunosensor based on gold nanoparticles for direct detection of atrazine. Sens Actuators B Chem 191:408–414. https://doi.org/10.1016/j.snb.2013.10.033

Ma J, Lee SMY, Yi C, Li CW (2017) Controllable synthesis of functional nanoparticles by microfluidic platforms for biomedical applications-a review. Lab Chip 17(2):209–226. https://doi.org/10.1039/C6LC01049K

Malvern Ltd. (2011) "Zeta potential: an introduction in 30 minutes." In: Zetasizer Nano Serles Technical Note. MRK654-01, vol 2. p 1–6. http://scholar.google.com/scholar?hl=en&btnG=Search&q=intitle:Zeta+Potential+An+Introduction+in+30+Minutes#0. Accessed 3 Jan 2023

McFarland AD, Haynes CL, Mirkin CA, Van Duyne RP, Godwin HA (2004) Color my nanoworld. J Chem Educ 81(4):544A. https://doi.org/10.1021/ed081p544a

Mello AJ, De MH, Llewellyn Lancaster N, Welton T, Wootton RCR (2004) Precise temperature control in microfluidic devices using Joule heating of ionic liquids. Lab Chip 4(5):417–419. https://doi.org/10.1039/b405760k

Mukherjee P, Patra CR, Ghosh A, Kumar R, Sastry M (2002) Characterization and catalytic activity of gold nanoparticles synthesized by autoreduction of aqueous chloroaurate ions with fumed silica. Chem Mater 14(4):1678–1684. https://doi.org/10.1021/cm010372m

Niikura K, Matsunaga T, Suzuki T, Kobayashi S, Yamaguchi H, Orba Y, Kawaguchi A et al (2013) Gold nanoparticles as a vaccine platform: influence of size and shape on immunological responses in vitro and in vivo. ACS Nano 7(5):3926–3938. https://doi.org/10.1021/nn3057005

Paquin F, Rivnay J, Salleo A, Stingelin N, Silva-Acuña C (2015) Multiphase microstructures drive exciton dissociation in neat semicrystalline polymeric semiconductors. J Mater Chem C 3(41):10715–10722. https://doi.org/10.1039/C5TC02043C

Park JW, Shumaker-Parry JS (2014) Structural study of citrate layers on gold nanoparticles: role of intermolecular interactions in stabilizing nanoparticles. J Am Chem Soc 136(5):1907–1921. https://doi.org/10.1021/ja4097384

Salazar-González JA, González-Ortega O, Rosales-Mendoza S (2015) Gold nanoparticles and vaccine development. Expert Rev Vaccines 14(9):1197–1211. https://doi.org/10.1586/14760584.2015.1064772

Sasidharan A, Monteiro-riviere NA (2015) Biomedical applications of gold nanomaterials: opportunities and challenges. Wires Nanomed Nanobiotechnol 7:779–796. https://doi.org/10.1002/wnan.1341

Schianti JN, Cerize NPN, Oliveira AM, Derenzo S, Góngora-Rubio MR (2013) 3-D LTCC microfluidic device as a tool for studying nanoprecipitation. J Phys Conf Ser. https://doi.org/10.1088/1742-6596/421/1/012012

Shafique MF, Robertson ID (2009) Rapid prototyping of LTCC microwave circuits using laser machining. In: IEEE MTT-S international microwave symposium digest. p 469–72. https://doi.org/10.1109/MWSYM.2009.5165735.

Singh P, Santosh Pandit VRSS, Mokkapati AG, Ravikumar V, Mijakovic I (2018) Gold nanoparticles in diagnostics and therapeutics for human cancer. Int J Mol Sci. https://doi.org/10.3390/ijms19071979

Sista R, Hua Z, Thwar P, Sudarsan A, Srinivasan V, Eckhardt A, Pollack M, Pamula V (2008) Development of a digital microfluidic platform for point of care testing. Lab Chip 8(12):2091–2104. https://doi.org/10.1039/b814922d

Thiele M, Soh JZE, Knauer A, Malsch D, Stranik O, Müller R, Csáki A, Thomas Henkel J, Köhler M, Fritzsche W (2016) Gold nanocubes—direct comparison of synthesis approaches reveals the need for a microfluidic synthesis setup for a high reproducibility. Chem Eng J 288:432–440. https://doi.org/10.1016/j.cej.2015.12.020

Uppal MA, Kafizas A, Ewing MB, Parkin IP (2013) The room temperature formation of gold nanoparticles from the reaction of cyclohexanone and auric acid; a transition from dendritic particles

to compact shapes and nanoplates. J Mater Chem A 1(25):7351–7359. https://doi.org/10.1039/c3ta11546a
Uson L, Sebastian V, Arruebo M, Santamaria J (2016) Continuous microfluidic synthesis and functionalization of gold nanorods. Chem Eng J 285:286–292. https://doi.org/10.1016/j.cej.2015.09.103
Vasudev A, Kaushik A, Jones K, Bhansali S (2013) Prospects of low temperature co-fired ceramic (LTCC) based microfluidic systems for point-of-care biosensing and environmental sensing. Microfluid Nanofluid 14(3–4):683–702. https://doi.org/10.1007/s10404-012-1087-3
Wagner J, Kirner T, Mayer G, Albert J, Köhler JM (2004) Generation of metal nanoparticles in a microchannel reactor. Chem Eng J 101(1–3):251–260. https://doi.org/10.1016/j.cej.2003.11.021
Wang P, Wang X, Wang L, Hou X, Liu W, Chen C (2015) Interaction of gold nanoparticles with proteins and cells. Sci Technol Adv Mater 16(3):34610. https://doi.org/10.1088/1468-6996/16/3/034610
Weng Chen Hsun, Huang Chih Chia, Yeh Chen Sheng, Lei Huan Yao, Lee Gwo Bin (2008) Synthesis of hexagonal gold nanoparticles using a microfluidic reaction system. J Micromech Microeng. https://doi.org/10.1088/0960-1317/18/3/035019
Whitesides GM (2006) The origins and the future of microfluidics. Nature 442(7101):368–373. https://doi.org/10.1038/nature05058
Wu H, Ji X, Zhao L, Yang S, Xie R, Yang W (2012) Shape evolution of citrate capped gold nanoparticles in seeding approach. Coll Surf A Physicochem Eng Aspects 415:174–179. https://doi.org/10.1016/j.colsurfa.2012.09.031
Wuithschick M, Birnbaum A, Witte S, Sztucki M, Vainio U, Pinna N, Rademann K, Emmerling F, Kraehnert R, Polte J (2015) Turkevich in new robes: key questions answered for the most common gold nanoparticle synthesis. ACS Nano 9(7):7052–7071. https://doi.org/10.1021/acsnano.5b01579
Xu L, Wang X, Wang W, Sun M, Choi WJ, Kim JY, Hao C et al (2022) Enantiomer-dependent immunological response to chiral nanoparticles. Nature 601(7893):366–373. https://doi.org/10.1038/s41586-021-04243-2
Ye Z, Wang Ke, Lou M, Jia X, Fengyun Xu, Ye G (2020) Consecutive synthesis of gold nanobipyramids with controllable morphologies using a microfluidic platform. Microfluid Nanofluid 24(5):1–8. https://doi.org/10.1007/s10404-020-02345-3
Zhang L, Widera G, Bleecher S, Zaharoff DA, Mossop B, Rabussay D (2003) Accelerated immune response to DNA vaccines. DNA Cell Biol 22(12):815–822. https://doi.org/10.1089/104454903322625028
Zhang J, Song F, Lin S, Liu S, Liu Y (2016) Tunable fluorescence lifetime of Eu-PMMA films with plasmonic nanostructures for multiplexing. Opt Express 24(8):8228. https://doi.org/10.1364/oe.24.008228

Authors and Affiliations

Natália Cristina Dalibera[1,2] · Aline Furtado Oliveira[3] · Adriano Rodrigues Azzoni[2]

✉ Natália Cristina Dalibera
nataliacd@ipt.br

[1] Unidade de Negócios Bionanomanufatura, Laboratório de Processos Químicos e Tecnologia de Partículas, Instituto de Pesquisas Tecnológicas do Estado de São Paulo - IPT, Av. Prof. Almeida Prado, Nº 532, Butantã, São Paulo, SP 05508-901, Brazil

[2] Departamento de Engenharia Química, Escola Politécnica, Universidade de São Paulo, Av. Prof. Luciano Gualberto, Trav. 3, Nº 380, Butantã, São Paulo, SP 05508-900, Brazil

[3] Instituto de Pesquisas Tecnológicas do Estado de São Paulo - IPT, Av. Prof. Almeida Prado, Nº 532, Butantã, São Paulo, SP, 05508-901, Brazil